Widespread brain parenchymal HMGB1 and NF-KB neuroinflammatory responses upon cortical spreading depolarization in familial hemiplegic migraine type 1 mice

Dehghani, A.; Phisonkunkasem, T.; Ozcan, S.Y.; Dalkara, T.; Maagdenberg, A.M.J.M. van den; Tolner, E.A.; Karatas, H.

Neurobiology of Disease 156 (2021) 105424

Contents lists available at ScienceDirect

Neurobiology of Disease

journal homepage: www.elsevier.com/locate/ynbdi

Widespread brain parenchymal HMGB1 and NF-κB neuroinflammatory responses upon cortical spreading depolarization in familial hemiplegic migraine type 1 mice

Anisa Dehghani [a,b,*], Thas Phisonkunkasem [b], Sinem Yilmaz Ozcan [a], Turgay Dalkara [a], Arn M.J. M. van den Maagdenberg [b,c], Else A. Tolner [b,c], Hulya Karatas [a,*]

[a] Institute of Neurological Sciences and Psychiatry, Hacettepe University, Ankara, Turkey
[b] Department of Human Genetics, Leiden University Medical Center, Leiden, the Netherlands
[c] Department of Neurology, Leiden University Medical Center, Leiden, the Netherlands

ARTICLE INFO

Keywords:
HMGB1
NF-κB
NMDA receptor
Excitability
Neuron
Astrocyte

ABSTRACT

Neuroinflammatory changes involving neuronal HMGB1 release and astrocytic NF-κB nuclear translocation occur following cortical spreading depolarization (CSD) in wildtype (WT) mice but it is unknown to what extent this occurs in the migraine brain. We therefore investigated in familial hemiplegic migraine type 1 (FHM1) knock-in mice, which express an intrinsic hyperexcitability phenotype, the extent of neuroinflammation without and after CSD. CSD was evoked in one hemisphere by pinprick (single CSD) or topical KCl application (multiple CSDs). Neuroinflammatory (HMGB1, NF-κB) and neuronal activation (pERK) markers were investigated by immunohistochemistry in the brains of WT and FHM1 mutant mice without and after CSD. Effects of NMDA receptor antagonism on basal and CSD-induced neuroinflammatory changes were examined by, respectively, systemically administered MK801 and ifenprodil or topical MK801 application. In FHM1 mutant mice, CSD caused enhanced neuronal HMGB1 release and astrocytic NF-κB nuclear translocation in the cortex and subcortical areas that were equally high in both hemispheres. In WT mice such effects were only pronounced in the hemisphere in which CSD was induced. Neuroinflammatory responses were associated with pERK expression indicating neuronal activation. Upon CSD, contralateral cortical and striatal HMGB1 release was reduced by topical application of MK801 in the hemisphere contralateral to the one in which CSD was induced. This study reveals that neuroinflammatory activation after CSD is widespread and extends to the contralateral hemisphere, particularly in brains of FHM1 mutant mice. Effective blockade of CSD-induced neuroinflammatory responses in the contralateral hemisphere in FHM1 mice by local NMDA receptor antagonism suggests that neuronal hyperexcitability-related neuroinflammation is relevant in migraine pathophysiology, but possibly also other neurological disorders in which spreading depolarization is involved.

1. Introduction

Neuroinflammation in the central nervous system typically occurs as an adaptive reaction of the brain to noxious stimuli such as infection or tissue injury and plays an important role in the pathophysiology of various brain disorders (Dendrou et al., 2016; Gilhus and Deuschl, 2019; Xanthos and Sandkuhler, 2014). Cortical spreading depolarization (CSD), the probable underlying cause of the migraine aura (Lauritzen, 1994; Ayata and Lauritzen, 2015), is a slowly propagating wave of neuronal and glial cell depolarization that causes a short-lasting (few minutes) ionic, metabolic and vascular brain perturbation known to act as a trigger of such mild neuroinflammation (Karatas et al., 2013). Experimentally induced CSD by pinprick or topical KCl application to the cortex in one hemisphere was shown to activate a

Abbreviations: CSD, cortical spreading depolarization; DC, direct-current; FHM1, Familial hemiplegic migraine type 1; HMGB1, high mobility group box 1; KCl, potassium chloride; KI, knock-in; NF-κB, Nuclear Factor of the κ-chain in B-cells; NMDA, *N*-methyl-D-aspartate; PFA, paraformaldehyde; Panx1, pannexin-1; pERK, phospho extracellular signal-regulated kinases; PET/MRI, Positron emission tomography–magnetic resonance imaging; PVDF, polyvinylidene difluoride; SDS-PAGE, sodium dodecyl sulphate-polyacrylamide; WT, wildtype.

* Corresponding author at: Institute of Neurological Sciences and Psychiatry, Hacettepe University, Ankara, Turkey.
E-mail addresses: A.Dehghani_Mohammadi@lumc.nl (A. Dehghani), hulyak@hacettepe.edu.tr (H. Karatas).

https://doi.org/10.1016/j.nbd.2021.105424
Received 7 December 2020; Received in revised form 4 April 2021; Accepted 8 June 2021
Available online 10 June 2021

neuroinflammatory cascade in wildtype (WT) mice (Karatas et al., 2013). In this cascade, CSD causes opening of neuronal Pannexin-1 (Panx1) channels and caspase-1 activation that subsequently trigger neuronal release of high mobility group box 1 (HMGB1) protein, the innate 'alarmin' molecule, and is followed by translocation of nuclear factor-κB (NF-κB) from the cytoplasm to the nucleus in astrocytes. These consequences were pronounced in the hemisphere in which CSD was induced, and occurred particularly in the cortex. However, Panx1 activation was also detected to some extent ipsilaterally and contralaterally in the dentate gyrus and contralaterally in the cortex (Karatas et al., 2013). This contralateral activation appears surprising as a CSD wave in WT mice typically does not propagate to the contralateral hemisphere, at least in anesthetized rodents (Charles and Brennan, 2009; Bolay et al., 2019). This raises the interesting possibility that excitatory volleys triggered at the onset of CSD may spread to contralateral brain areas to activate neuronal Panx1 channels and the downstream inflammatory cascade. Clinical evidence for migraine-related widespread neuroinflammatory changes comes from a recent clinical PET/MRI study which showed the uptake of inflammatory radiotracer in cortical as well as subcortical areas of both hemispheres in patients suffering from frequent migraine with aura attacks (Albrecht et al., 2019).

To investigate brain neuroinflammatory responses in the migraine context, we here used transgenic mouse models of familial hemiplegic migraine type 1 (FHM1) (for review Ferrari et al., 2015; Dehghani and Karatas, 2019) harboring the R192Q (van den Maagdenberg et al., 2004) or S218L (van den Maagdenberg et al., 2010) missense mutation in the α_{1A} subunit of neuronal voltage-gated $Ca_V2.1$ channels have a gain of $Ca_V2.1$ channel activity leading to intrinsically enhanced cortical excitatory (glutamatergic) neurotransmission (Vecchia et al., 2014, 2015) and an increased susceptibility to experimentally induced CSD (van den Maagdenberg et al., 2004; Eikermann-Haerter et al., 2009; Tottene et al., 2009). We hypothesized that neuroinflammatory responses may be more pronounced in FHM1 mutant mice, both in the naïve state and following CSD, given that naïve animals exhibit astrocytic activation in the cortex and microglial activation in the cortex and striatum (Magni et al., 2019), and one day after CSD, mutant animals have a distinct molecular inflammatory signature in the ipsilateral cortex (Eising et al., 2017). Since CSD can propagate extensively to subcortical areas in FHM1 mutant in contrast to WT mice (Eikermann-Haerter et al., 2011), CSD-induced inflammatory responses may also be more widespread in FHM1 mutants. To investigate our hypothesis, and provide a mechanistic link between genetically determined brain hyperexcitability, CSD and susceptibility to neuroinflammation, we assessed the extent of the neuroinflammatory response based on changes in HMGB1 and NF-κB in brains of naïve (unstimulated) FHM1 mutant and WT mice and after CSD. Our data demonstrate a widespread neuroinflammatory response (shown by neuronal HMGB1 release and astrocytic NF-κB nuclear translocation) in naïve mice and in response to CSD. Our findings also provide a link between the hyperexcitability phenotype in FHM1 mutants and brain neuroinflammation based on regional colocalization of neuroinflammatory marker HMGB1 with neuronal pERK expression and effective blockage of the neuroinflammatory profile in FHM1 mutants with an NMDA receptor antagonist.

2. Material and methods

2.1. Animals

Two- to four-month-old female wildtype (WT), transgenic homozygous *Cacna1a* FHM1 R192Q and heterozygous *Cacna1a* FHM1 S218L knock-in (KI) mice ("R192Q or S218L mutant mice") were used. FHM1 mutant mice were generated by introducing the respective human pathogenic *CACNA1A* missense mutation in the orthologous mouse *Cacna1a* gene using a gene targeting approach (van den Maagdenberg et al., 2004; van den Maagdenberg et al., 2010). Mice were housed under a 12-h light/dark cycle under standard housing conditions with food and water available ad libitum. All experimental procedures were carried out in accordance with recommendations of the European Communities Council Directive (2010/63/EU) and were approved by the ethical committees of Hacettepe University and Leiden University Medical Center, and carried out in accordance with ARRIVE guidelines. All efforts were made to minimize animal suffering.

2.2. Study size

A total of 46 mice were used for the experiments. Although mean differences between the outcome parameters were expected to be relatively high up to 40% (Karatas et al., 2013), previous immunohistology experiments for HMGB1, and NF-κB, and Western blot experiments for HMGB1 and NF-κB indicated variation. To detect a difference of 40% between groups with an expected variation of 20–25% for immunohistological and Western blot readouts, power of 80% and a significance level of 5%, the estimated sample size was 4–5 per group for the HMGB1, NF-κB and pERK immunohistological and 5–6 per group for the HMGB1 and NF-κB Western blot experiments.

2.3. Induction of a single CSD by pinprick

To induce a single CSD, mice underwent a pinprick applied through a drilled burr hole. To this end, mice were placed into a stereotaxic frame under urethane (1.25 g/kg, i.p.) and xylazine (10 mg/kg, i.p) anesthesia and allowed to breathe spontaneously under nasal oxygen support (2 L/min) with a body temperature maintained at 37 ± 0.1 °C by a rectal probe and homeothermic blanket control unit. Recording of direct-current (DC) and alternating current (AC) potentials was started prior to drilling, using two Ag-AgCl pellet electrodes (1 mm diameter) placed over the thinned skull of the right (and for a subset of experiments also the left) parietal bone (1.5 mm posterior to bregma, 2 mm mediolateral). Signals were digitized, displayed, and stored on a computer by a data acquisition and analysis system (Powerlab 16/35; AD Instruments, Bella Vista, Australia). A burr hole was drilled over the right primary motor cortex (1.3 mm anterior and 1 mm lateral to bregma) using a high-speed drill while cooling with saline and without removing the dura mater. Next, a needle (26-gauge) was inserted inside the burr hole at ~2 mm depth for 1 s to induce a single CSD event. Sham controls ('drilled group') underwent the same drilling procedure but without the subsequent pinprick. DC-recordings confirmed the occurrence of a single CSD in the right cortex and absence of CSD in the contralateral left cortex and in drilled controls. A CSD was defined as a transient negative DC-shift of >5 mV measured at two locations with a delay, associated with a decrease in AC amplitude. 30 min following CSD, animals were sacrificed by transcardial perfusion via a short (1-min) heparinized saline infusion followed by 4% paraformaldehyde (PFA) for 4 min, to avoid previously reported perfusion-induced hypoxic stress on neurons and its effect on HMGB1 release (Dehghani et al., 2018). Naïve (non-operated) control mice were anesthetized following deep anesthesia by i.p. 1 mg/g chloral hydrate injection followed by perfusion.

2.4. Induction of multiple CSDs by KCl application

To induce multiple CSDs, mice were anesthetised and a burr hole was drilled over the right motor cortex as described above. About 7–10 CSDs were induced by topical application of KCl on the dura overlaying the right primary motor cortex for 1 h. To this end, a cotton ball soaked in 1 M KCl was placed in the burr hole and refreshed every 10 min, while CSDs were recorded using Ag-AgCl pellet electrodes on the skull as described for pinprick-induced CSD. Sham experiments consisted of the same procedure with application of 1 M NaCl, which does not induce CSDs.

2.5. Immunohistochemistry

Whole brains were quickly removed after transcardial perfusion (as described above). Tissue was post-fixed in 4% PFA overnight and cryoprotected in 30% sucrose in PBS for two days. Coronal sections were cut at 20 μm on a cryostat and incubated 24 h at 4 °C with primary antibodies of rabbit polyclonal pERK (1:200; Cell Signaling, Danvers, MA) rabbit polyclonal HMGB1 (1:200; Abcam, Cambridge, MA), mouse monoclonal NeuN (1:200; Chemicon International, Temecula, CA), mouse monoclonal NF-κB (P65) (1:200; Cell Signaling) and rabbit polyclonal S100-beta (1:200; Abcam). This was followed by a 90-min incubation at RT with secondary goat anti-rabbit Cy2 (1:200; Jackson ImmunoResearch, West Grove, PA) and goat anti-mouse Cy3 (1:200; Jackson ImmunoResearch) antibodies. For S100-beta and NF-κB double-staining first antigen retrieval was performed for 10 min at 80 °C in 10 mM sodium citrate buffer in 0.05% Tween (pH 6). All immunolabeled sections were mounted in 1:1 glycerol:PBS medium containing 12.5 mg/mL sodium azide and 1 μL/mL Hoechst-33,258, and examined by epifluorescence and laser-scanning confocal microscopy.

2.6. Subcellular fractionation

Whole brains from mice from the multiple CSD experiments were quickly removed after a 1-h KCl application and dissected rapidly (within ~1 min) in frontal and parietal cortices, striatum and thalamus for both the ipsilateral hemisphere, in which CSD was induced, and the contralateral hemisphere, separately. Tissues were prepared for nuclear and cytoplasmic fractionation using NE-PER Nuclear and Cytoplasmic Extraction Reagents (Thermo-Fisher Sci, Waltham, MA) according to the supplier's instructions. Protein extracts were stored at −80 °C until used for Western blotting.

2.7. Western blotting

For Western blotting of brain samples, the amount of protein was quantified using the Pierce BCA Protein Assay Kit (Thermo-Fisher Sci). For each sample, 30 μg protein was loaded and run on a sodium dodecyl sulphate (SDS)-polyacrylamide (SDS-PAGE) gel and subsequently transferred to polyvinylidene difluoride (PVDF) membranes. Primary antibody incubation (α-NF-κB 1:1000, Santa Cruz, Dallas, TX; α-Histone-3 1:2000, Cell Signaling; α-β3-Tubulin 1:2500, Sigma, St. Louis, MO) was performed overnight at 4 °C, followed by secondary antibody (horseradish peroxidase conjugated anti-rabbit IgG 1:5000; Cell Signaling) incubation for 1 h at RT. α-Histone-3 and α-β3-Tubulin proteins were used as nuclear and cytoplasmic fraction loading controls. Images were captured by a Kodak (Rochester, NY) 4000MM image station and analysed with Carestream (Rochester, NY) Molecular Imaging Software.

2.8. Quantification of immunoreactivity for HMGB1 release, NF-κB nuclear translocation and pERK activation

HMGB1 release - HMGB1-label[1]led neurons were quantified at 200× magnification in each specific mouse brain region, i.e. in the right hemisphere in superficial layers of the primary motor cortex and somatosensory cortex, the striatum, and ventral part of the thalamus, leading to four randomly picked sections from all area; the same was performed for the left hemisphere; per mouse (n = 5 mice), a total of 400–500 NeuN-positive cells were analysed in each of the selected brain regions. A NeuN-positive/HMGB1-negative cell was counted as neuron with 'total HMGB1 release', based on the knowledge that in healthy WT mouse brain tissue, the majority of NeuN-positive neurons are HMGB1-immunopositive (Karatas et al., 2013). A NeuN-positive/HMGB1-positive signal was regarded as 'no HMGB1 release'. *NF-κB nuclear translocation* - NF-κB quantification was performed at 400× magnification on four randomly picked images obtained from each mouse brain area, as indicated above. A total of 70–100 astrocytes were analysed in each of the selected brain regions per mouse (n = 4 mice). To assess the number of astrocytes with NF-κB translocated to the nucleus, S100-beta-positive cells with nuclear NF-κB (confirmed by Hoechst-33,258) were counted as fraction of the total number of S100-beta-positive cells. *pERK activation* - Four randomly picked sections from both frontal and posterior brain regions were examined at 200× magnification for pERK-positive cells. The same areas examined for HMGB1 release were quantified. A total of 500–600 cells were analysed in each of the selected brain regions per mouse (n = 4 mice).

Fluorescent-labelled sections were examined under a wide-field fluorescence or laser-scanning confocal microscope with appropriate filter sets. All quantifications were done in ImageJ version 1.52q. Quantification of HMGB1 release, NF-κB nuclear translocation and pERK expression was performed by two researchers (A.D. and T.P.), who were blinded for genotype and treatment; for all quantifications the data sets of the two researchers were averaged.

2.9. Pharmacological interventions

NMDA receptor antagonist MK801 (1 mmol/L in aCSF; Sigma) or vehicle was applied topically to the corresponding contralateral location in the *left* cortex (0.15 mm posterior and 0.65 mm lateral to bregma) 1 h before a CSD was induced by pinprick in the *right* somatosensory cortex (0.15 mm posterior and 0.65 mm lateral to bregma). Mice were transcardially perfused as described above 30 min following a single CSD. In separate groups of naïve mice either MK801 (0.6 mg/kg, in saline) or vehicle was injected i.p. twice a day with an 8-h interval for a period of 3 days (Zuo et al., 2006), or ifenprodil (20 mg/kg, dissolved in distilled water), another NMDA receptor antagonist, or vehicle was injected i.p. once (Schidlitzki et al., 2017) without inducing CSD. Mice were transcardially perfused (Dehghani et al., 2018) 1 h after the last injection.

2.10. Statistical analysis

For a graphical presentation of the data, mean values were presented using bar charts with error bars representing the standard error of mean values. Since the data were non-normally distributed, median and interquartile range (IQR: 25th–75th percentiles) were also calculated and presented for HMGB1 and NF-κB analysis in Table 1. Comparisons between more than two independent groups were made with the Kruskal-Wallis test, followed by the post hoc pairwise comparisons with Mann-Whitney *U* test utilizing Bonferroni correction. All p-values are two-tailed, and a p-value <0.05 was considered statistically significant, except for post hoc analyses, in which a p-value was calculated according to Bonferroni correction. Statistical analysis was performed using GraphPad Prism 5 (GraphPad Software, La Jolla, CA) and IBM SPSS Statistics version 23 (IBM, Armonk, NY).

3. Results

3.1. Increase in the number of neurons without HMGB1 immunoreactivity following a single CSD is more pronounced in the ipsilateral hemisphere in wildtype mice

Total neuronal HMGB1 release was assessed from the percentage of neurons (NeuN-positive) without HMGB1 immunoreactivity, in the primary motor and somatosensory cortices, striatum and ventral part of the thalamus of WT mice that were subjected to a single, pinprick-induced CSD (Fig. 1A, B). In mice that underwent anesthesia and cardiac perfusion, but no drilling or CSD ('naïve group'), HMGB1 release was low (<5%), regardless of the region studied (Fig. 1C). In mice that underwent drilling ('drilled group') but no CSD, HMGB1 release was

[1] If siganling is with 1 "l" than labelled is also with 1 "l" so "labeled"

Table 1
Median and interquartile values of the various outcome parameters of the different experiments for HMGB1 release and NF-κB translocation in FHM1 mutant and WT mice in naïve, drilled and CSD conditions; CSD: cortical spreading depolarization; Cx: cortex; WT: wild-type.

HMGB1 analysis	25% Percentile	Median	75% Percentile		25% Percentile	Median	75% Percentile
Ipsi Motor cx R192Q Naïve	6.20	6.65	7.625	Ipsi Motor cx WT Naïve	3.42	4.30	4.50
Ipsi Motor cx R192Q Drilled	11.58	13.60	18.48	Ipsi Motor cx WT Drilled	8.40	9.80	11.50
Ipsi Motor cx R192Q CSD	34.50	36.00	55.50	Ipsi Motor cx WT CSD	33.50	36.00	45.00
Ipsi Motor cx S218L Naïve	17.00	17.80	22.20	Contra Motor cx WT Naïve	2.72	3.15	4.10
Contra Motor cx R192Q Naïve	6.10	6.85	7.75	Contra Motor cx WT Drilled	7.40	7.75	8.92
Contra Motor cx R192Q Drilled	18.90	20.00	21.30	Contra Motor cx WT CSD	9.00	12.00	17.50
Contra Motor cx R192Q CSD	30.50	38.00	57.00	Ipsi Striatum WT Naïve	3.95	4.15	4.50
Contra Motor cx S218L Naïve	8.10	9.20	13.53	Ipsi Striatum WT Drilled	7.82	8.65	9.40
Ipsi Striatum R192Q Naïve	8.60	8.70	8.80	Ipsi Striatum WT CSD	61.00	72.00	92.50
Ipsi Striatum R192Q Drilled	21.90	25.00	25.70	Contra Striatum WT Naïve	3.30	4.15	4.77
Ipsi Striatum R192Q CSD	40.75	52.50	68.00	Contra Striatum WT Drilled	5.12	8.40	9.05
Ipsi Striatum S218L Naïve	8.05	10.40	12.38	Contra Striatum WT CSD	23.50	25.00	29.00
Contra Striatum R192Q Naïve	5.87	7.95	8.67	Ipsi Somatosensory cx WT CSD	27.00	29.00	59.50
Contra Striatum R192Q Drilled	18.00	19.80	20.00	Contra Somatosensory cx WT CSD	20.50	23.00	47.00
Contra Striatum R192Q CSD	39.75	52.50	63.75	Ipsi Thalamus WT CSD	67.50	78.00	86.00
Contra Striatum S218L Naïve	7.12	7.75	9.2	Contra Thalamus WT CSD	31.50	70.00	82.50
Ipsi Somatosensory cx R192Q CSD	17.50	25.00	59.50	Ipsi Thalamus R192Q CSD	73.25	81.00	92.50
Contra Somatosensory cx R192Q CSD	17.75	24.00	61.75	Contra Thalamus R192Q CSD	80.50	83.50	94.75
NF-κB analysis	25% Percentile	Median	75% Percentile		25% Percentile	Median	75% Percentile
Ipsi Motor cx WT Naïve	5.595	6.790	9.06	Ipsi Motor cx R192Q Naïve	8.575	10.35	19.78
Ipsi Motor cx WT CSD	85.93	87.70	92.03	Ipsi Motor cx R192Q CSD	92.10	96.50	99.05
Contra Motor cx WT Naïve	5.52	6.190	7.70	Contra Motor cx R192Q Naïve	8.50	8.94	14.34
Contra Motor cx WT CSD	43.25	74.40	75.78	Contra Motor cx R192Q CSD	72.19	93.78	94.10
Ipsi Striatum WT Naïve	4.71	4.94	5.20	Ipsi Striatum R192Q Naïve	8.98	10.76	14.61
Ipsi Striatum WT CSD	88.73	93.75	96.83	Ipsi Striatum R192Q CSD	95.70	96.50	97.90
Contra Striatum WT Naïve	4.20	4.68	5.16	Contra Striatum R192Q Naïve	9.41	9.75	16.01
Contra Striatum WT CSD	38.50	64.65	82.33	Contra Striatum R192Q CSD	77.20	89.90	96.45

increased in both the ipsilateral (i.e. the hemisphere in which CSD was induced) and contralateral motor cortex as well as ipsilateral striatum (Fig. 1C). A single CSD led to a marked increase in HMGB1 release in both hemispheres compared to the naïve and drilled groups but the increase was much higher in the ipsilateral (motor cortex: $p = 0.008$ and striatum: $p = 0.008$) than the respective contralateral brain areas (Fig. 1C). For the somatosensory cortex ($p = 0.063$) and ventral thalamus ($p = 0.114$), however, the increase after CSD was similarly large for both hemispheres (Fig. 1D). Of note, after CSD, HMGB1 release in ipsilateral striatal and ventral thalamic areas was particularly pronounced with close to 80% of neurons showing release, whereas in ipsilateral cortical areas release was observed in approximately 40% of neurons.

3.2. NF-κB nuclear translocation in astrocytes following a single CSD is more pronounced in the ipsilateral hemisphere of wildtype mice

Translocation from cytoplasm to the nucleus, thereby indicating activation, of NF-κB in astrocytes reflects a neuroinflammatory response following CSD (Karatas et al., 2013). The number of astrocytes with NF-κB nuclear expression was increased in the motor cortex and striatum of both hemispheres of WT mice upon a single CSD compared to naïve mice, but, as for HMGB1, the increase was more pronounced in the ipsilateral brain areas (Fig. 1E, F).

3.3. Increase in the number of neurons without HMGB1 immunoreactivity following a single CSD is equally strong in both hemispheres of FHM1 mutant mice

Next, we investigated whether neuroinflammatory responses upon a single CSD are more pronounced in FHM1 mutant mice (i.e. in mice harboring the R192Q or the S218L missense mutation in the α_{1A} subunit of $Ca_V2.1$ Ca^{2+} channels), which show a hyperexcitability phenotype that is most pronounced in the S218L mutant (for review Ferrari et al., 2015). In naïve FHM1 mutant mice, i.e. animals that did not undergo drilling or CSD, higher levels of neuronal HMGB1 release, based on the number of neurons without HMGB1 immunoreactivity, were observed for all investigated brain areas when compared to WT mice ($p = 0.028$; graph not shown). HMGB1 release in the various brain areas was similarly high between R192Q and S218L mutant mice, except for the release in ipsilateral striatum, which was higher in S218L mutants (Fig. 2A). These results show that the low basal level of HMGB1 release seen in WT mice is already enhanced in the mutants by the presence of the FHM1 mutation. In R192Q mutant mice that also underwent drilling, but no CSD, HMGB1 release was further increased in ipsilateral motor cortex ($p = 0.028$). In R192Q mutants, in contrast to WT mice, neuronal HMGB1 release after a single CSD was pronounced bilaterally in the motor and somatosensory cortices, striatum and the ventral thalamus, i.e. with no difference between hemispheres (Fig. 2A, B). In the thalamus, bilateral release was more pronounced compared to striatum ($p = 0.029$ for both ipsi- and contralateral side).

3.4. Astrocytic NF-κB nuclear translocation following a single CSD is equally pronounced in both hemispheres of FHM1 mutant mice

Next, we investigated whether bilateral neuroinflammatory responses in FHM1 mutant mice also involve astrocytic NF-κB nuclear translocation, assessed here in motor cortex and striatum. Translocation in naïve R192Q mutant mice was small but higher for both brain areas compared to WT ($p = 0.029$; graph not shown). Translocation in mutant mice was enhanced following a single CSD when compared to naïve animals ($p = 0.028$; Fig. 2C) with no difference between the ipsi- and contralateral hemisphere.

To extend the immunohistochemistry finding of nuclear translocation of NF-κB following a single pinprick-induced CSD in cortical and subcortical regions, we also assessed effects of CSD on NF-κB nuclear translocation in brain tissue using Western blotting, in FHM1 S218L mutant and WT mice. FHM1 S218L mutants were chosen for the experiments since naïve mice of this strain exhibit a more pronounced neuronal HMGB1 release (by immunoreactivity) compared to naïve mice of the R192Q strain (Fig. 2C). To maximize chances of observing effects of CSD on NF-κB nuclear translocation at the whole tissue level, we assessed effects of *multiple* CSD events instead of a single one, similarly to what was done for WT mice in Karatas et al. (2013). For

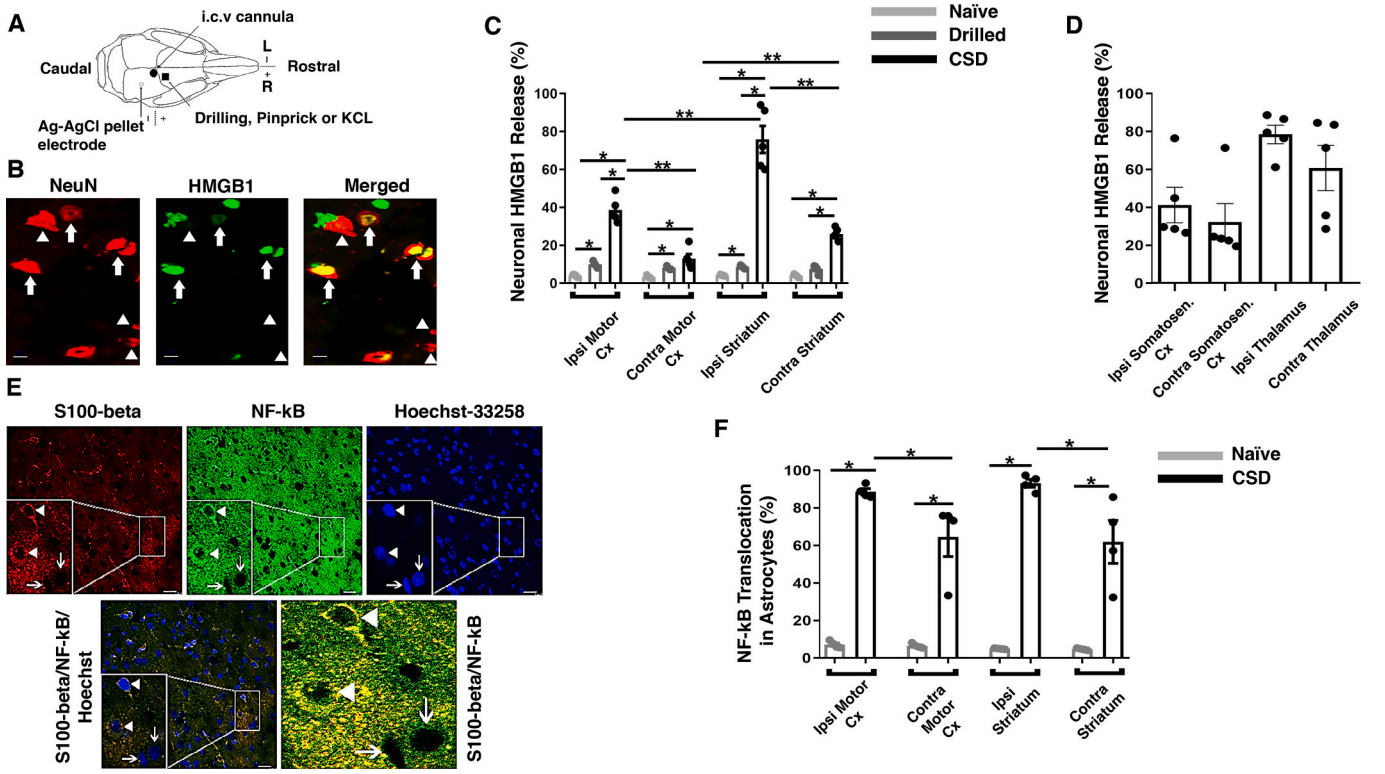

Fig. 1. HMGB1 release and NF-κB translocation in brains of naïve wildtype mice (WT) and after CSD. (A) Schematic showing the location of (i) the craniotomy for pinprick- or KCl-induced CSDs in the motor cortex and (ii) non-invasive DC recording over the visual cortex via an extracranial Ag-AgCl pellet electrode. (B) Representative confocal images of the somatosensory cortex showing colocalization of neuronal nuclei (NeuN, in red) with HMGB1 signal (in green). NeuN-positive/HMGB1-negative cells (arrowheads) were counted as total HMGB1 release. NeuN-positive/HMGB1-positive cells (arrows) were counted as no release in HMGB1. Scale bar 10 μm. (C) Neuronal HMGB1 release in the motor cortex and striatum in naive, drilled and CSD groups; n = 5 for all groups. (D) Bilateral neuronal HMGB1 release in the somatosensory cortex and thalamic area 30 min following CSD; n = 5 for all groups. (E) Representative confocal images of superficial layers of the motor cortex of a WT mouse following CSD showing NF-κB translocation from the cytoplasm to the nucleus in astrocytes (arrowheads in all images). Inset shows two astrocytes (arrowheads, S100-beta positive, in red) adjacent to two neurons (arrows, S100-beta negative). NF-κB immunoreactivity is shown in green, which is visible in the nuclei of astrocytes (arrowheads in NF-κB and merged images). In neurons, NF-κB is visible as a rim in the cytoplasm but not in nuclei (arrows in NF-κB image). Hoechst-33,258 (blue) as a nuclear marker shows the colocalization of NF-κB in nuclei of astrocytes (arrowheads, merged image). Scale bars: 10 μm. Images were taken from 20-μm-thick coronal sections by laser scanning confocal microscope. (F) NF-κB translocation from cytoplasm to nucleus in astrocytes in the motor cortex and striatum in naive and CSD groups, assessed 30 min following CSD; n = 4 for all groups. Ipsi: the hemisphere in which drilling or CSD induction was performed; Contra: the hemisphere contralateral to the site of drilling or CSD induction; Somatosen: somatosensory; Cx: cortex. Bars show standard error of the mean (SEM). *p ≤ 0.05; **p ≤ 0.01. (For interpretation of the references to colour in this figure legend, the reader is referred to the web version of this article.)

induction of multiple CSDs, 1 M KCl was applied topically to the cortex for 1 h, resulting in 7–10 CSD events. Sham experiments consisted of the same procedure with application of 1 M NaCl, which did not induce CSDs. S218L mutant mice showed a similar extent of NF-κB nuclear translocation in the CSD and sham groups, with sham values of S218L mutant mice being higher than in WT mice for both ipsilateral cortical regions (combined motor and somatosensory cortex; p = 0.026; Fig. 2D) and contralateral subcortical regions (combined striatum and thalamus; p = 0.004; Fig. 2E). Multiple CSDs led to an increase in NF-κB nuclear translocation in S218L mutant mice compared to WT mice in contralateral subcortical regions (p = 0.007). Translocation in the contralateral subcortical regions in WT mice was increased in the CSD group compared to the sham group (p = 0.022).

3.5. Bilaterally increased pERK activation after CSD only in FHM1 mutant mice

To investigate the involvement of neuronal activation in the spread of neuroinflammation responses, we compared the number of pERK-positive cells in both hemispheres of WT and R192Q mutant mice. The number of pERK-positive cells in the motor cortex (p = 0.028; Fig. 3A,E) and striatum (p = 0.028; Fig. 3B,F) was already higher for both hemispheres in naïve R192Q mutant compared to WT mice. Following a single CSD, bilaterally increased pERK activation was observed in both the cortical and striatal areas in R192Q mutant mice, whereas in WT mice pERK activation was only enhanced in the ipsilateral hemisphere in these regions (Fig. 3C–F). The bilateral pERK activation observed in cortical and subcortical brain regions in naïve mice and following CSD (Fig. 4A) parallels the observed bilateral inflammatory profile of neuronal HMGB1 release in cortical and subcortical areas in naïve FHM1 mutant mice and following CSD (Fig. 4B).

3.6. NMDA receptor antagonism reduces contralateral HMGB1 release upon CSD and in naïve FHM1 mutant mice

Given the pronounced (sub)cortical neuroinflammatory responses following CSD in the contralateral hemisphere in FHM1 mutant mice, we investigated whether such responses might be transmitted by CSD-induced neuronal activity through transcallosal fibers that connect the sensorimotor areas of both hemispheres (Hoffmeyer et al., 2007). Through such a mechanism, CSDs in one hemisphere can exert effects that extend into the other hemisphere. To investigate whether blocking neuronal communication between hemispheres would prevent the CSD-related contralateral inflammatory response, we topically applied the non-competitive NMDA receptor antagonist MK801 or vehicle on the contralateral motor cortex 1 h before a single CSD was induced in the

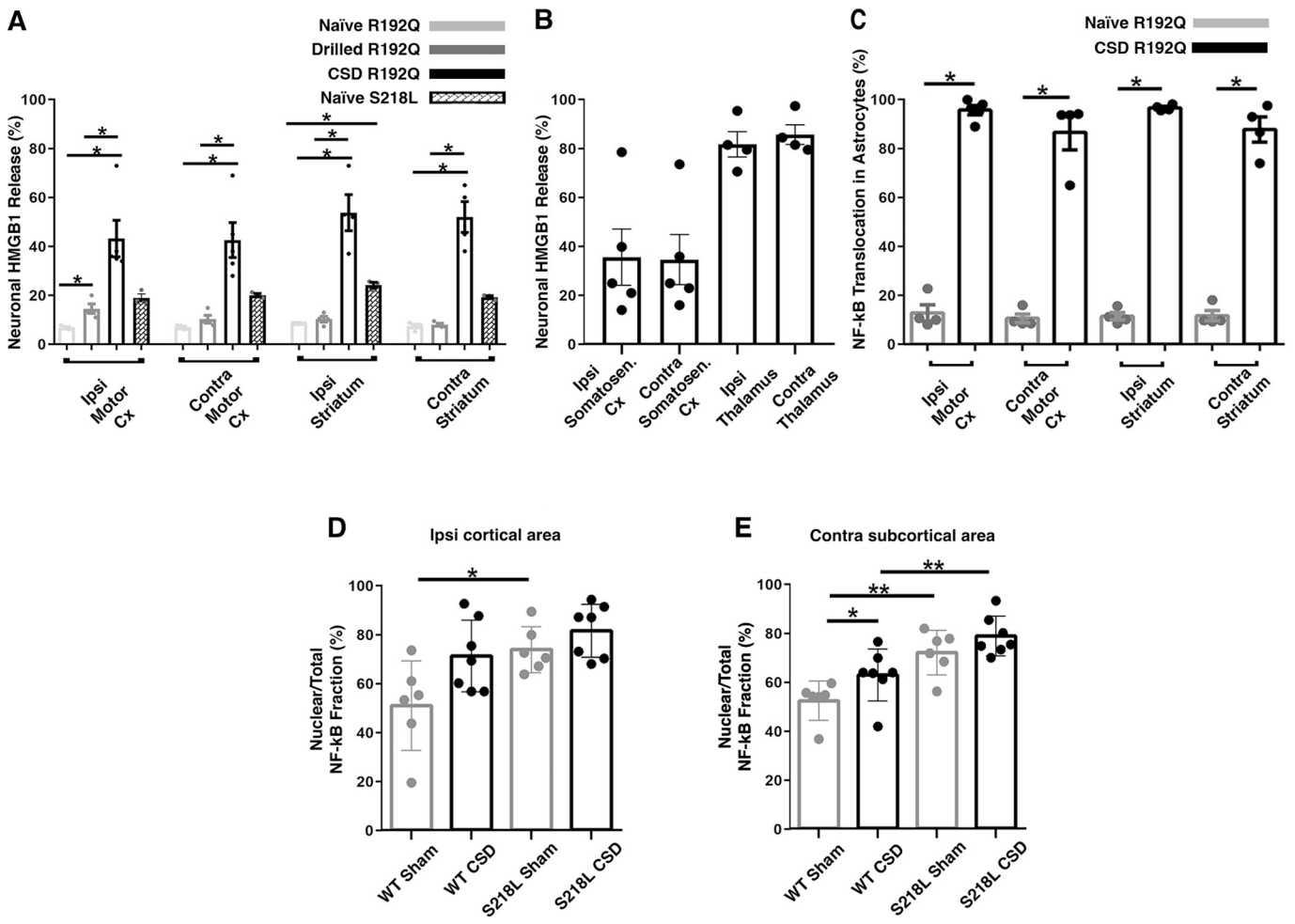

Fig. 2. HMGB1 release and NF-κB translocation in naïve FHM1 mutant mice and after CSD. (A) Neuronal HMGB1 release in motor cortex and striatum in naïve, drilled and CSD groups; n = 5 R192Q homozygous mice for all groups. (B) Neuronal HMGB1 release in the somatosensory cortex and thalamic area in the CSD group; n = 5 R192Q homozygous mice for all groups. (C) NF-κB translocation from cytoplasm to nucleus in astrocytes in motor cortex and striatum in naïve and CSD groups; n = 4 R192Q homozygous mice for all groups. (D, E) NF-κB translocation from cytoplasm to nucleus in astrocytes shown by nuclear sub-fractionation Western blotting of (D) the ipsilateral cortex and (E) contralateral sub-cortical areas (i.e. including striatum and thalamus) of the brains of WT and heterozygous S218L mutant mice immediately after a 1-h induction of multiple CSDs by topical 1 M KCl application. For sham group saline was applied; n = 6–7 for all groups. Ipsi: the hemisphere in which drilling or CSD induction was performed; Contra: the hemisphere contralateral to the site of drilling or CSD induction; Somatosen: somatosensory; Cx: cortex. Bars show standard error of the mean (SEM). *p ≤ 0.05; **p ≤ 0.01.

ipsilateral hemisphere (Fig. 5A). While topical MK801 application on the left motor cortex did not influence the induction of CSD on the right motor cortex compared to vehicle or untreated controls, it decreased neuronal HMGB1 release in the contralateral (left) motor cortex to 16.6 ± 4.4% in the MK801 group compared to 53.0 ± 4.1% in the vehicle-treated group (p = 0.029; Fig. 5B–D). To assess whether NMDA receptor antagonism also normalizes neuronal basal HMGB1 release in naïve R192Q mutant mice, MK801 or the NR2B-selective NMDA receptor antagonist ifenprodil was administered systemically, without inducing CSD. For both MK801- and ifenprodil-treated mice, HMGB1 release seemed lower in the motor cortex and striatum of both hemispheres, but the reduction was only statistically significant in the ifenprodil-treated mice for the left (p = 0.029) and right motor cortex (p = 0.029) and right striatum (p = 0.051) (Fig. 5E).

4. Discussion

Here we show that a single CSD can cause a profound widespread brain neuroinflammatory response, as evidenced by increased neuronal HMGB1 release and astrocytic NF-κB nuclear translocation, which are equally strong in both hemispheres of FHM1 mutant mice. In contrast, a single CSD event induced in WT brains causes less pronounced neuroinflammatory responses that are weaker in the contralateral compared to the ipsilateral hemisphere in which CSD was induced. A low level of basal neuronal HMGB1 release and astrocytic NF-κB nuclear translocation is observed in naïve FHM1 mutant, but not WT mice, suggesting that FHM1 transgenic mice are intrinsically susceptible to neuroinflammation, which can be profoundly aggravated by a relatively mild (transient) perturbation such as CSD. Local blockage of NMDA receptors by topical application of MK801 to the contralateral hemisphere reduced the CSD-induced neuroinflammatory response in both cortical and subcortical areas in this hemisphere. This suggests that the intrinsically enhanced cortical glutamatergic neurotransmission in FHM1 mutant mice (Vecchia et al., 2014, 2015) plays an important role in the observed widespread inflammatory responses after CSD in mutant mice. In addition, the observation in FHM1 mutant mice that remote expression of neuroinflammatory markers coincided with pERK expression, a marker for enhanced neuronal activity, in the same areas, suggests involvement of a neuronally-mediated spread. Further studies are needed to uncover the precise neuronal networks involved. The pronounced bilateral HMGB1 release observed for both WT and FHM1 mutant mice in the somatosensory cortex, and the high levels of

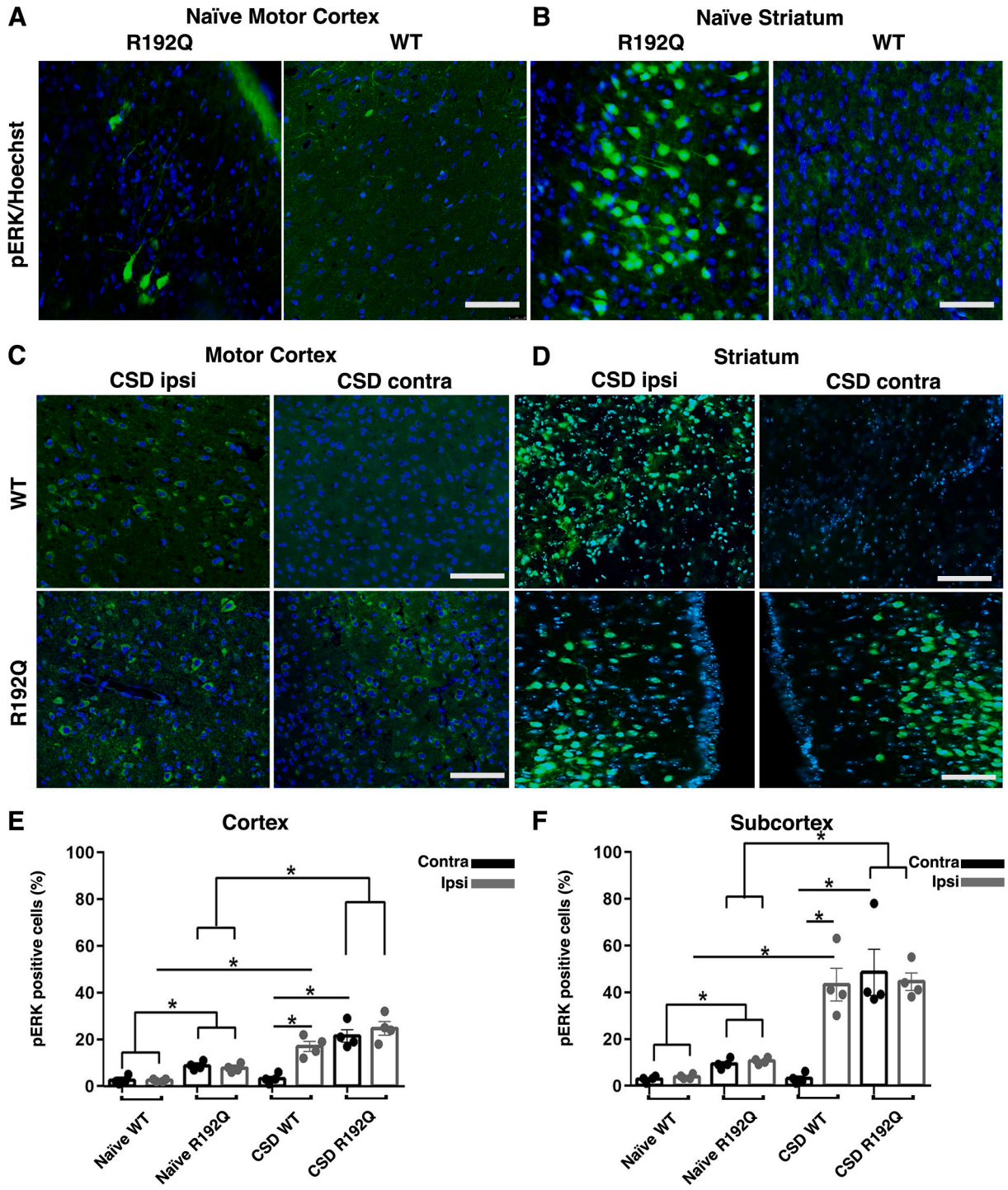

Fig. 3. Increased pERK expression in the brains of FHM1 mutant compared to wildtype (WT) mice. (A) Representative fluorescent images of pERK signal (green) in the motor cortex and (B) striatum of unstimulated, naïve mice. Cell nuclei are labelled with Hoechst-33,258 (blue). (C, D) Representative fluorescent images showing pERK expression after CSD in motor cortex (C) and striatum (D). Scale bars: 50 μm. Images were taken from 20-μm-thick coronal sections by laser scanning confocal microscope. (E, F) Quantification of the number of pERK positive cells in the motor cortex (E) and striatum (F). Bars show standard error of the mean (SEM); *$p \leq 0.05$; $n = 4$ for all groups. (For interpretation of the references to colour in this figure legend, the reader is referred to the web version of this article.)

thalamic HMGB1 release in both WT and mutants seem in line with the convergence of cortical inputs (including from the somatosensory cortex) to the thalamus (Sherman, 2016).

A recent PET/MRI study provided supportive clinical data for the CSD-induced widespread neuroinflammation (Albrecht et al., 2019), which we observed in the mouse migraine mutant brain. In that study, brain scans with ^{11}C-PBR28, a marker of inflammatory glial activation, were obtained from migraine with aura patients and healthy controls. Migraineurs had increased neuroimmune activation in widespread brain areas including thalamus, primary/secondary somatosensory and insular cortices, which are involved in pain processing. This activation was thought to be specific to neuroinflammation in migraine (Bu et al., 2020) and not relevant to pain in general since patients suffering from chronic lumbar pain did not show such tracer uptake in pain processing areas (Loggia et al., 2015). The signal intensity was also positively associated with the frequency of migraine with aura attacks (Albrecht

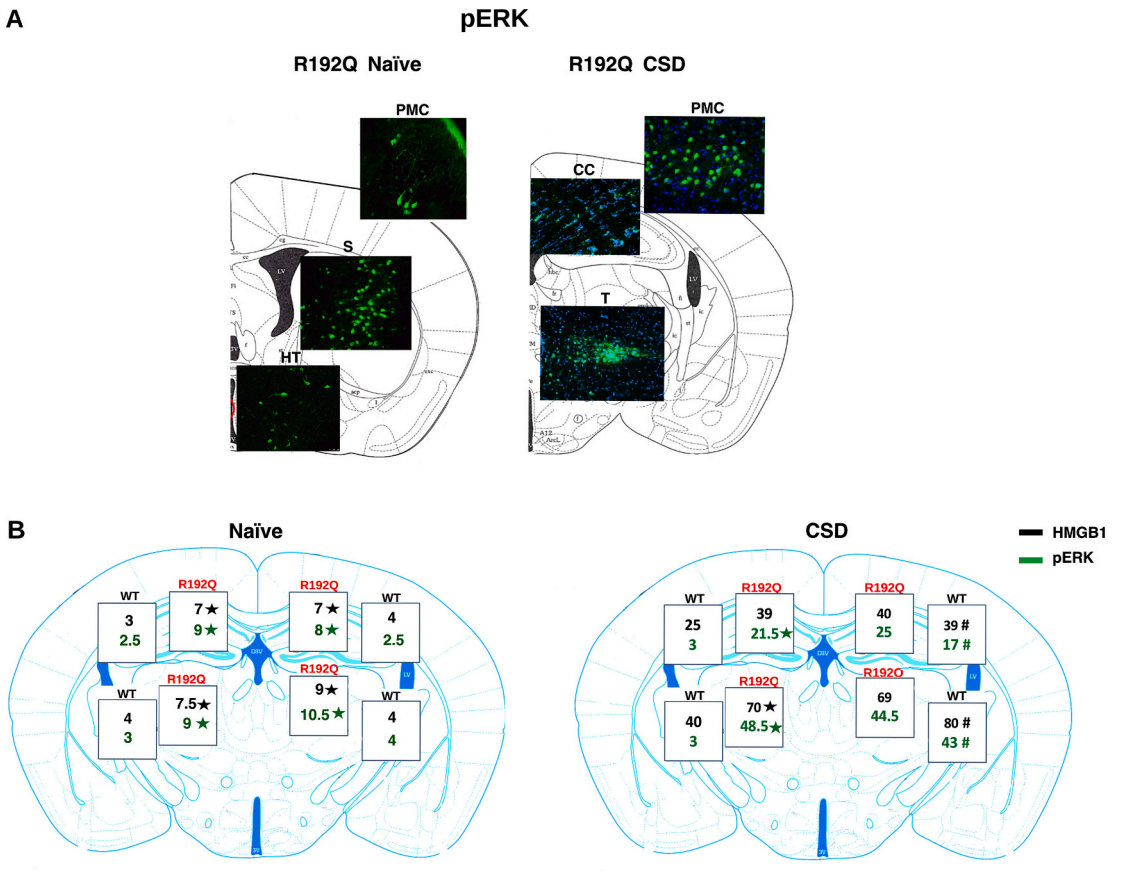

Fig. 4. Comparison of anatomical areas showing pERK activation and neuronal HMGB1 release in the brains of naïve FHM1 mutant and wildtype (WT) mice and 30 min following CSD. (A) Representative fluorescent images of pERK signal (green) in FHM1 mutant mice without and after CSD shown in a schematic of primary motor cortex (PMC), somatosensory cortex (SC), striatum (S), thalamus (T) and hypothalamus (HT). (B) Schematic comparison of the percentage amount of neuronal HMGB1 release (black numbers) and pERK positivity (green numbers) in brains of naïve FHM1 mutant (R192Q homozygous) and WT mice and after CSD (comparison of cortex and thalamus) (n = 4). Anatomical schemes adapted from Paxinos and Franklin, 2019 Significance level ($p < 0.05$) is shown for both neuronal HMGB1 release (black font) and pERK expression (green font) for genotype (*; i.e. WT vs FHM1 mutant, for the particular anatomical area) and laterality (#; i.e. right vs left hemisphere at a similar anatomical area). (For interpretation of the references to colour in this figure legend, the reader is referred to the web version of this article.)

et al., 2019), which suggests that in migraine with aura with recurrent attacks repeated exposure of the brain to CSD during the aura phase may induce a bilateral and widespread neuroinflammatory activity, similar to what we have observed in FHM1 mutant mice.

CSD is known to activate the neuroinflammatory cascade in the brain areas it invades (Karatas et al., 2013; Eising et al., 2017; Asanuma and Okuda, 1962). However, widespread presence of the inflammatory response in both hemispheres in FHM1 mutant mice cannot be attributed to propagation of CSD out of the cortex where it was triggered, as previous studies on FHM1 mutant mice have shown that CSD does not propagate to the contralateral hemisphere, except - under specific circumstances - for thalamus, despite robust penetration into ipsilateral subcortical areas (Eikermann-Haerter et al., 2011). Alternatively, contralateral neuroinflammatory responses may be mediated by intense axonal volleys that typically fire at the beginning of CSD wave before depression of electrical activity (Herreras et al., 1994). These volleys arrive at the contralateral corresponding cortex area through corpus callosum (Hoffmeyer et al., 2007) and are likely relayed to downstream subcortical areas. Intense excitatory firing, as occurring during epileptiform discharges, has the capacity to activate Panx1 channels (hence, the activation of the downstream inflammatory pathway) secondary to overactivation of NMDA receptors (Thompson et al., 2008). Supporting this possibility, we were able to suppress the neuroinflammatory profile in the contralateral cortex and striatum by locally inhibiting NMDA receptors by MK801 at the level of the contralateral (non-CSD) cortex of mutant mice. This mechanism could also underlie the contralateral neuroinflammatory responses in WT mice, although they were less pronounced compared to FHM1 mutant mice. In rats, NMDA receptor activation was shown to underlie CSD-induced Panx1 activation ipsilaterally, but contralateral effects were not studied (Bu et al., 2020). In epilepsy animal models, HMGB1 activation is implicated in the propagation of seizures, which was suggested to involve HMGB1-mediated signaling leading to potentiation of NMDA-mediated Ca^{2+} influx into neurons (Paudel et al., 2019). It is possible that inhibition of NMDA-receptor may have contributed to suppression of the bilateral neuroinflammatory profiles following CSD by preventing HMGB1-mediated spread of neuronal activity.

While cortical injury in the right primary motor cortex caused by pinprick cannot be excluded for our immunohistochemical studies, this seems unlikely to underlie the observed HMGB1 and NF-κB changes observed following CSD. First, CSD-induced HMGB1 release was pronounced not only in the right motor cortex but also in the right somatosensory cortex in which no pinprick was made. Second, the increase in NF-κB nuclear translocation following pinprick-induced CSD was confirmed by Western blotting following induction of multiple CSDs by topical KCl application. The view that CSD-related neuroinflammatory responses are not dependent on the CSD induction method is also supported by a recent study that demonstrated increased expression of several cortical neuroinflammatory markers following a single as well as multiple CSDs induced by non-invasive optogenetics as well as

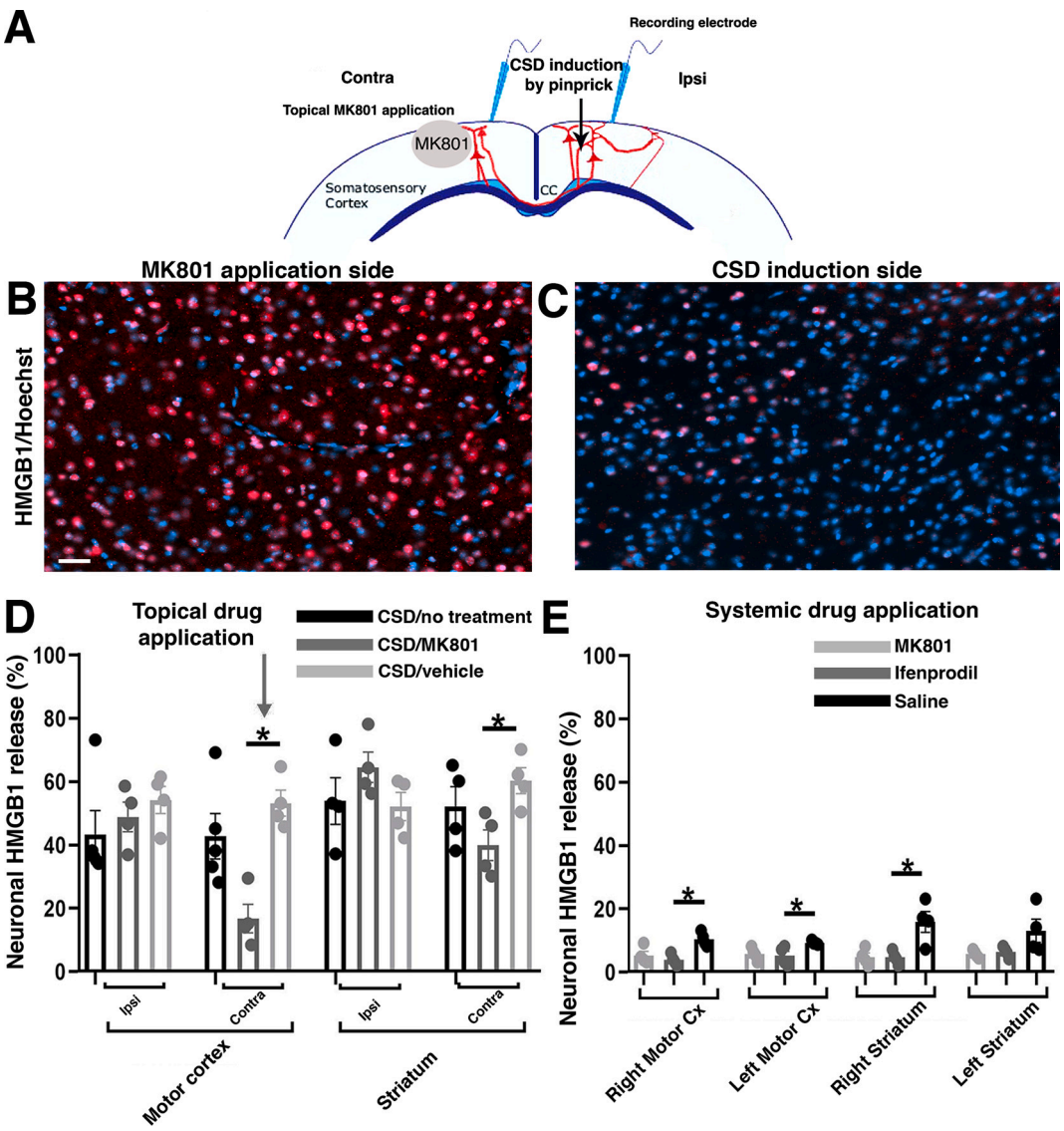

Fig. 5. Effect of NMDA receptor antagonists on neuronal HMGB1 release in brains of FHM1 mutant mice following CSD induction (B—D) and in the naïve state (E). (A) Schematic of the experimental approach for the CSD-induction experiments with the location of the DC-recording electrodes, MK801 application and CSD induction sites by pinprick. MK801 (or saline in the sham group) was topically applied on the cortex contralateral to the site of CSD induction, which did not influence the ipsilateral CSD induction by pinprick. (B, C) Representative confocal images showing HMGB1 signal in the contralateral (B) and ipsilateral cortex (C, site of CSD induction). HMGB1 signal is shown in red and nuclei are labelled with Hoechst-33,258 (blue). Note the limited number of HMGB1-positive cells, indicating HMGB1. release, in the ipsilateral cortex, which is reduced in the contralateral cortex by topical MK801 application. Scale bar = 50 μm. (D) Neuronal HMGB1 release in the motor cortex and striatum of brains of FHM1 mutants following CSD induction for untreated, MK-801-treated, and vehicle-treated groups; n = 4 R192Q homozygous mice for all groups. (E) Basal (naïve) neuronal HMGB1 release (without CSD) in the right and left motor cortex and striatum after acute (one i.p. injection of ifenprodil) or chronic (i.e. 2 times daily for 3 consecutive days an i.p. injection of MK801) administration of an NMDA receptor antagonist; *p ≤ 0.05; n = 4 R192Q homozygous mice for all groups. Saline was applied i.p. in sham groups (n = 4). Cx: cortex. Bars show standard error of the mean (SEM). (For interpretation of the references to colour in this figure legend, the reader is referred to the web version of this article.)

minimally invasive KCl application through thinned skull (Takizawa et al., 2020).

Besides the MK801 effects, knowledge that FHM1 mutants are prone to an enhanced level of cortical glutamatergic transmission also supports the involvement of dysregulated excitatory transmission in the widespread character of inflammatory responses in these animals. Concomitant pERK activation in remote areas, to which CSD does not propagate, further suggests that neuronal overactivation in cortical and subcortical areas in both hemispheres has contributed to the widespread bilateral neuroinflammatory changes in FHM1 mutants. Interestingly, in the absence of CSD, naïve FHM1 mutants also had a low level of basal neuroinflammation suggesting that spontaneous glutamatergic activity may reach the threshold for activating NMDA receptors and subsequent induction of Panx1 channel opening. This is supported by the observed suppression of the basal neuroinflammation following systemically administered NMDA receptor antagonist ifenprodil.

Altogether, our findings point to a previously unrecognized pathophysiological mechanism: a local perturbation (i.e. CSD in one hemisphere) can lead to a widespread inflammatory response in the brain. This response is intensified by enhanced glutamatergic transmission as present in FHM1 mutant mice, which might also contribute to the exaggerated vulnerability to head trauma seen in FHM patients (Ferrari et al., 2015). Supporting this possibility, FHM1 mutant mice showed an inflammatory response to simple drilling of the cranium that was not occurring for WT mice. The brain of migraine with aura patients may also be prone to widespread and intense neuroinflammatory responses

to CSD (i.e. underlying the aura phase), as suggested by the previously mentioned PET/MRI study in migraine with aura patients (Albrecht et al., 2019).

In conclusion, the global aggravation of neuro-glial communication involving (enhanced) glutamatergic transmission as the mechanism of neuroinflammatory changes indicated by our study, brings about novel therapeutic opportunities based on targeting neuroinflammatory pathways, in particular NMDA receptors and HMGB1 protein. It is an exciting possibility that such strategies may represent an effective therapeutic intervention for migraine, but also other neurological disorders in which spreading depolarization is involved, and may eventually lead to a biomarker of neuroinflammation for diagnosis and drug development.

Author contribution

A.D., A.M.J.M.v.d.M., E.A.T., T.D. and H.K. conceptualized and designed the study. A.D., T.P., S.Y.O and H.K. performed the experiments. A.D., T.P., E.A.T. and H.K analysed the data. A.D. wrote the manuscript with contributions from A.M.J.M.v.d.M, T.D., E.A.T., and H. K.

Declaration of competing interest

The authors declare no conflicts of interest.

Acknowledgements

The authors wish to thank Mesut Firat and Sandra van Heiningen for technical support.

Funding

This work was supported by grants from Hacettepe University Scientific Research Projects Unit (grant no. THD-2018-15457 to H.K.), International Headache Society (IHS) Fellowship Award (to A.D.), the European Union "Euroheadpain" grant (grant no. 602633 to A.M.J.M.v.d.M.), Centre for Medical Systems Biology (CMSB) in the framework of the Netherlands Genomics Initiative (NGI) (to A.M.J.M.vdM), Marie Curie IAPP Program BRAINPATH (grant no. 612360 to A.M.J.M.v.d.M. & E.A.T.).

Sample CRediT author statement

Anisa Dehghani: Conceptualization, Data curation, Formal analysis, Funding acquisition, Investigation, Methodology, Project administration, Visualization, Writing - original draft. Thas Phisonkunkasem: Data curation, Formal analysis Sinem Yilmaz Ozcan: Data curation Turgay Dalkara: Conceptualization, Writing - review & editing. Arn M. J. M. van den Maagdenberg: Conceptualization, Funding acquisition, Writing - review & editing. Else A. Tolner: Conceptualization, Funding acquisition, Writing - review & editing. Hulya Karatas: Conceptualization, Data curation, Formal analysis, Funding acquisition, Investigation, Supervision, Writing - review & editing.

References

Albrecht, D.S., Mainero, C., Ichijo, E., Ward, N., Granziera, C., Zürcher, N.R., Akeju, O., Bonnier, G., Price, J., Hooker, J.M., Napadow, V., Loggia, M.L., Hadjikhani, N., 2019. Imaging of neuroinflammation in migraine with aura: a [^{11}C] PBR28 PET/MRI study. Neurology 92, e2038–e2050.

Asanuma, H., Okuda, O., 1962. Effects of transcallosal volleys on pyramidal tract cell activity of cat. J. Neurophysiol. 25, 198–208.

Ayata, C., Lauritzen, M., 2015. Spreading depression, spreading depolarizations, and the cerebral vasculature. Physiol. Rev. 95, 953–993.

Bolay, H., Vuralli, D., Goadsby, P.J., 2019. Aura and head pain: relationship and gaps in the translational models. J, Headache Pain 20, 94.

Bu, F., Nie, L., Quinn, J.P., Wang, M., 2020. Sarcoma family kinase-dependent pannexin-1 activation after cortical spreading depression is mediated by NR2A-containing receptors. Int. J. Mol. Sci. 21, 1269.

Charles, A., Brennan, K.C., 2009. Cortical spreading depression - new insights and persistent questions. Cephalalgia 29, 1115–1124.

Dehghani, A., Karatas, H., 2019. Mouse models of familial hemiplegic migraine for studying migraine pathophysiology. Curr. Neuropharmacol. 17, 961–973.

Dehghani, A., Karatas, H., Can, A., Erdemli, E., Yemisci, M., Eren-Kocak, E., Dalkara, T., 2018. Nuclear expansion and pore opening are instant signs of neuronal hypoxia and can identify poorly fixed brains. Sci. Rep. 8, 1–13.

Dendrou, C.A., McVean, G., Fugger, L., 2016. Neuroinflammation-using big data to inform clinical practice. Nat. Rev. Neurol. 12, 685–698.

Eikermann-Haerter, K., Dileköz, E., Kudo, C., Savitz, S.I., Waeber, C., Baum, M.J., Ferrari, M.D., van den Maagdenberg, A.M.J.M., Moskowitz, M.A., Ayata, C., 2009. Genetic and hormonal factors modulate spreading depression and transient hemiparesis in mouse models of familial hemiplegic migraine type 1. J. Clin. Invest. 119, 99–109.

Eikermann-Haerter, K., Yuzawa, I., Qin, T., Wang, Y., Baek, K., Kim, Y.R., Hoffmann, U., Dilekoz, E., Waeber, C., Ferrari, M.D., van den Maagdenberg, A.M., 2011. Enhanced subcortical spreading depression in familial hemiplegic migraine type 1 mutant mice. J. Neurosci. 31, 5755–5763.

Eising, E., Shyti, R., 't Hoen, Peter A.C., Vijfhuizen, L.S., Huisman, S.M.H., Broos, L.A.M., Mahfouz, A., Reinders, M.J.T., Ferrari, M.D., Tolner, E.A., de Vries, B., van den Maagdenberg, A.M.J.M., 2017. Cortical spreading depression causes unique dysregulation of inflammatory pathways in a transgenic mouse model of migraine. Mol. Neurobiol. 54, 2986–2996.

Ferrari, M.D., Klever, R.R., Terwindt, G.M., Ayata, C., van den Maagdenberg, A.M.J.M., 2015. Migraine pathophysiology: lessons from mouse models and human genetics. Lancet Neurol. 14, 65–80.

Gilhus, N.E., Deuschl, G., 2019. Neuroinflammation-a common thread in neurological disorders. Nat. Rev. Neurol. 15, 429–430.

Herreras, O., Largo, C., Ibarz, J.M., Somjen, G.G., del Rio, R.M., 1994. Role of neuronal synchronizing mechanisms in the propagation of spreading depression in the in vivo hippocampus. J. Neurosci. 14, 7087–7098.

Hoffmeyer, H.W., Enager, P., Thomsen, K.J., Lauritzen, M.J., 2007. Nonlinear neurovascular coupling in rat sensory cortex by activation of transcallosal fibers. J. Cerebr. Blood F Met. 27, 575–587.

Karatas, H., Erdener, S.E., Gursoy-Ozdemir, Y., Lule, S., Eren-Koçak, E., Sen, Z.D., Dalkara, T., 2013. Spreading depression triggers headache by activating neuronal Panx1 channels. Science 339, 1092–1095.

Lauritzen, M., 1994. Pathophysiology of the migraine aura. The spreading depression theory. Brain 117, 199–210.

Loggia, M.L., Chonde, D.B., Akeju, O., Arabasz, G., Catana, C., Edwards, R.R., Hill, E., Hsu, S., Izquierdo-Garcia, D., Ji, R.R., Riley, M., 2015. Evidence for brain glial activation in chronic pain patients. Brain 138, 604–615.

Magni, G., Boccazzi, M., Bodini, A., Abbracchio, M.P., van den Maagdenberg, A.M.J.M., Ceruti, S., 2019. Basal astrocyte and microglia activation in the central nervous system of familial hemiplegic migraine type I mice. Cephalalgia 39, 1809–1817.

Paudel, Y.N., Angelopoulou, E., Piperi, C., Balasubramaniam, V.R., Othman, I., Shaikh, M.F., 2019. Enlightening the role of high mobility group box 1 (HMGB1) in inflammation: updates on receptor signalling. Eur. J. Pharmacol. 858, 172487.

Paxinos, G., Franklin, K.B., 2019. Paxinos and Franklin's the Mouse Brain in Stereotaxic Coordinates, fifth ed. Academic Press.

Schidlitzki, A., Twele, F., Klee, R., Waltl, I., Römermann, K., Bröer, S., Meller, S., Gerhauser, I., Rankovic, V., Li, D., Brandt, C., 2017. A combination of NMDA and AMPA receptor antagonists retards granule cell dispersion and epileptogenesis in a model of acquired epilepsy. Sci. Rep. 7, 1–19.

Sherman, S.M., 2016. Thalamus plays a central role in ongoing cortical functioning. Nat. Neurosci. 19, 533–541.

Takizawa, T., Qin, T., Lopes de Morais, A., Sugimoto, K., Chung, J.Y., Morsett, L., Mulder, I., Fischer, P., Suzuki, T., Anzabi, M., Böhm, M., 2020. Non-invasively triggered spreading depolarizations induce a rapid pro-inflammatory response in cerebral cortex. J. Cerebr. Blood F Met. 40, 1117–1131.

Thompson, R.J., Jackson, M.F., Olah, M.E., Rungta, R.L., Hines, D.J., Beazely, M.A., MacDonald, J.F., MacVicar, B.A., 2008. Activation of pannexin-1 hemichannels augments aberrant bursting in the hippocampus. Science 322, 1555–1559.

Tottene, A., Conti, R., Fabbro, A., Vecchia, D., Shapovalova, M., Santello, M., van den Maagdenberg, A.M.J.M., Ferrari, M.D., Pietrobon, D., 2009. Enhanced excitatory transmission at cortical synapses as the basis for facilitated spreading depression in CaV2. 1 knockin migraine mice. Neuron 6, 762–773.

van den Maagdenberg, A.M.J.M., Pietrobon, D., Pizzorusso, T., Kaja, S., Broos, L.A.M., Cesetti, T., van de Ven, R.C.G., Tottene, A., van der Kaa, J., Plomp, J.J., Frants, R.R., 2004. A Cacna1a knockin migraine mouse model with increased susceptibility to cortical spreading depression. Neuron 41, 701–710.

van den Maagdenberg, A.M.J.M., Pizzorusso, T., Kaja, S., Terpolilli, N., Shapovalova, M., Hoebeek, F.E., Barrett, C.F., Gherardini, L., Van De Ven, R.C.G., Todorov, B., Broos, L.A.M., Tottene, A., Gao, Z., Fodor, M., De Zeeuw, C.I., Frants, R.R., Plesnila, N., Plomp, J.J., Pietrobon, D., Ferrari, M.D., 2010. High cortical spreading depression susceptibility and migraine-associated symptoms in $Ca_V2.1$ S218L mice. Ann. Neurol. 67, 85–98.

Vecchia, D., Tottene, A., van den Maagdenberg, A.M.J.M., Pietrobon, D., 2014. Mechanism underlying unaltered cortical inhibitory synaptic transmission in contrast with enhanced excitatory transmission in $Ca_V2.1$ knockin migraine mice. Neurobiol. Dis. 69, 225–234.

Vecchia, D., Tottene, A., van den Maagdenberg, A.M.J.M., Pietrobon, D., 2015. Abnormal cortical synaptic transmission in $Ca_V2.1$ knockin mice with the S218L missense

mutation which causes a severe familial hemiplegic migraine syndrome in humans. Front Cell Neurosci. 17, 8.
Xanthos, D.N., Sandkuhler, J., 2014. Neurogenic neuroinflammation: inflammatory CNS reactions in response to neuronal activity. Nat. Rev. Neurosci. 15, 43–53.
Zuo, D.Y., Zhang, Y.H., Cao, Y., Wu, C.F., Tanaka, M., Wu, Y.L., 2006. Effect of acute and chronic MK-801 administration on extracellular glutamate and ascorbic acid release in the prefrontal cortex of freely moving mice on line with open-field behavior. Life Sci. 78, 2172–2178.